Traffic Jams, Gliders, and Bands in the Quest for Collective Motion of Self-Propelled Particles

Fernando Peruani,[1] Tobias Klauss,[2] Andreas Deutsch,[2] and Anja Voss-Boehme[2]

[1]*Max Planck Institute for the Physics of Complex Systems, Nöthnitzer Str. 38, 01187 Dresden, Germany*

[2]*Zentrum für Informationsdienste und Hochleistungsrechnen, Technische Universität Dresden, Zellescher Weg 12, 01069 Dresden, Germany*

(Received 21 October 2010; published 21 March 2011)

We study a simple swarming model on a two-dimensional lattice where the self-propelled particles exhibit a tendency to align ferromagnetically. Volume exclusion effects are present: particles can only hop to a neighboring node if the node is empty. Here we show that such effects lead to a surprisingly rich variety of self-organized spatial patterns. As particles exhibit an increasingly higher tendency to align to neighbors, they first self-segregate into disordered particle aggregates. Aggregates turn into traffic jams. Traffic jams evolve toward gliders, triangular high density regions that migrate in a well-defined direction. Maximum order is achieved by the formation of elongated high density regions—bands—that transverse the entire system. Numerical evidence suggests that below the percolation density the phase transition associated with orientational order is of first order, while at full occupancy it is of second order.

DOI: 10.1103/PhysRevLett.106.128101 PACS numbers: 87.18.Gh, 05.65.+b, 05.70.Ln, 87.10.Hk

Self-propelled particle (SPP) systems are found at all scales in nature. Examples in biology range from human crowds [1] and animal groups [2,3], down to insects [4,5], bacteria [6], and even to the microcellular scale with, e.g., the collective motion of microtubules driven by molecular motors [7]. SPP systems are not restricted to living systems. There are examples in nonliving matter, such as, for instance in driven granular media [8–10]. Interestingly, the statistical properties of the large-scale self-organized patterns emerging in SPP systems depend only on a few microscopic details: the symmetry associated to the self-propulsion mechanism of the particles, which can be either polar [11–13] or apolar [14], the symmetry of the velocity alignment mechanism, which can be either ferromagnetic [11,12] or nematic [13,14], and very importantly, the presence or absence of volume exclusion effects, as we are going to discuss here. In addition, the nature of the supporting space where the particles move plays also a crucial role: the dimension of the space, and whether this space is continuous [11–14] or discrete [15–18].

In this Letter, we focus on polar SPPs moving on a two-dimensional lattice that align their orientation, respectively, their moving direction, via a local ferromagnetic alignment mechanism. We explicitly model volume exclusion effects: nodes can be occupied at most by one particle. We show that such effects introduce a coupling between particle speed, local density and local alignment that lead to a surprisingly rich variety of self-organized spatial patterns unseen in previous swarming models. As particles exhibit an increasingly higher tendency to align to neighbors, the system passes through three distinct phases. For weak alignment strength, the system exhibits orientational disorder, while particles self-segregate, Fig. 1(a). Within this initial phase, there is a transition from a spatially homogeneous to an aggregate phase. The onset of orientational (polar) order marks the beginning of the second phase which is characterized by the emergence of locally ordered, high density regions: traffic jams, Fig. 1(b). As the tendency to align is enhanced, traffic jams evolve toward triangular high density aggregates that migrate in a well-defined direction. We refer to these dynamical traffic jams as gliders, Fig. 1(c). The third phase emerges when the particles self-organize into highly ordered, elongated, high density regions: bands, Fig. 1(d). In contrast to the traveling bands observed in off-lattice SPP models with ferromagnetic alignment [12], these bands are formed by particles aligned to the long axis of the band and are rather static.

We find evidence that the phase transition to orientational order is discontinuous below the percolation threshold. When the lattice is fully occupied, the system reduces to the classical planar Potts model and the phase transition to orientational order is undoubtedly of second order [19,20]. Previous lattice swarming models were found to exhibit a continuous phase transition from a homogeneous to a condensed phase in 1D [17,18], while in 2D, both, first and second-order transitions to orientational order have been claimed. Bussemaker *et al.* reported a second-order transition in a cellular automaton model with 4 moving directions [15], while Csahók and Vicsek found, for a lattice-gas model with 6 moving directions, a weakly-first-order transition to collective migration [16]. Here we show that all these phenomena occur in a minimal 2D lattice swarming model, but where in contrast to previous models the system dynamics is dominated by volume exclusion effects that lead to a completely novel spatial self-organization of particles.

Model.— Particles move on a two-dimensional lattice with periodic boundary conditions, and have four possible orientations: up, down, left, and right, whose associated

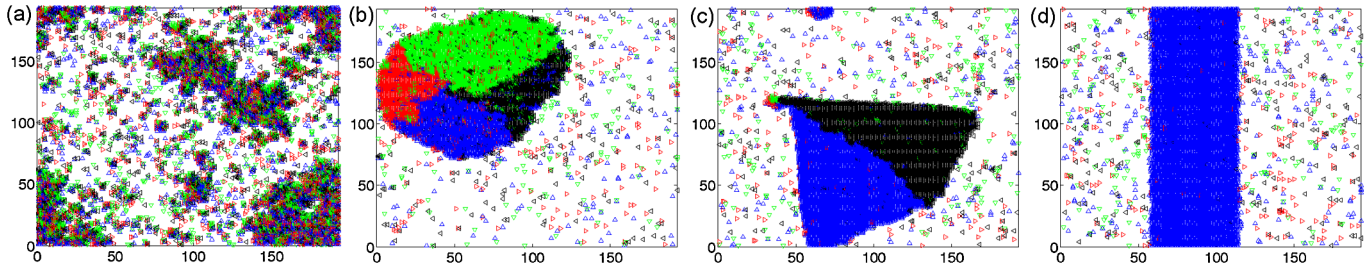

FIG. 1 (color online). Example of self-organized spatial patterns: (a) disordered aggregates, (b) traffic jams, (c) gliders, and (d) bands. Particle orientation is indicated by the orientation of the small triangles, and is also color-coded: right (red), left (black), down (green), and up (blue). Parameter values are indicated in Fig. 2.

vectors are $\mathbf{v}_1$, $\mathbf{v}_2$, $\mathbf{v}_3$, and $\mathbf{v}_4$, respectively. The state of a particle is given by its position on the lattice and its orientation. As it will become clear below, the orientation of a particle fully determines its moving direction. The particles are able to perform two actions: (i) they can change their orientation, and (ii) they can migrate in the direction given by their orientation. These actions have associated transition rates which specify the average number of events per time unit. Let us start out with the reorientation transition rate T_R that a particle at $\mathbf{x}$ with orientation $\mathbf{v}$ turns its orientation into direction $\mathbf{w}$:

$$T_R((\mathbf{x},\mathbf{v}) \to (\mathbf{x},\mathbf{w})) = \exp\Big(g \sum_{\mathbf{y}\in A(\mathbf{x})} \langle \mathbf{w}|\mathbf{V}(\mathbf{y})\rangle\Big), \quad (1)$$

where the sum runs over the nearest lattice neighbors of $\mathbf{x}$, represented by $A(\mathbf{x})$. The vector $\mathbf{V}(\mathbf{y})$ returns the orientation of the particle placed in node $\mathbf{y}$, if there is any, and the null vector otherwise. The symbol $\langle .|. \rangle$ indicates the inner product between two vectors, while g is a parameter which controls the alignment sensitivity. For positive g, Eq. (1) defines a stochastic ferromagnetic alignment mechanism. As result of this alignment, first nearest neighbor particles tend to be aligned.

The migration rate is defined in the following way:

$$T_M((\mathbf{x},\mathbf{v}) \to (\mathbf{y}=\mathbf{x}+\mathbf{v},\mathbf{v})) = \begin{cases} \upsilon_0 & \text{if node } \mathbf{y} \text{ is empty} \\ 0 & \text{if node } \mathbf{y} \text{ is occupied.} \end{cases} \quad (2)$$

Thus, a particle at position $\mathbf{x}$ and pointing in direction $\mathbf{v}$ migrates to the neighboring node $\mathbf{y} = \mathbf{x} + \mathbf{v}$ with a transition rate υ_0 as long as the node at $\mathbf{y}$ is empty. If the $\mathbf{y}$ node is occupied, the particle will not jump. The only action that is allowed to the particle in this situation is to change its orientation.

At this point, it is important to understand how this continuous-time process is simulated. Let us assume that at time t_0 the system is in a given state. Then, we compute the time at which the next event will take place in the system, i.e., we calculate t_1. Now we have to decide which is the event that will take place at time t_1. We choose at random one out of all the possible events that could take place, but we weight each of these events according to their associated transition rate, Eqs. (1) and (2). This procedure is an adaption of the classical Gillespie algorithm [21] to interacting particle systems [22].

Results.— We start by fixing the migration rate υ_0 and particle density d, and use g as control parameter. The degree of orientational order in the system at time t is characterized by the (global) orientation $m(t) = (1/N)|\sum_{\mathbf{x}} \mathbf{V}(\mathbf{x})|$, where N is the total number of particles in the system, the sum runs over all lattice sites, and $\mathbf{V}(\mathbf{x})$ is defined as above. Figure 2 shows the behavior of the mean orientation $\langle m \rangle$ as function of the alignment sensitivity g, with $\langle \ldots \rangle$ a temporal average taken once the system reaches the steady-state after a short transient. The system exhibits a phase transition to orientational order above a critical g^* for all densities, as long as $\upsilon_0 > 0$. Here we focus on $0 < d < d_p$, where d_p refers to the (site) percolation threshold in a 2D (square) lattice, $d_p \sim 0.59$. The system exhibits three phases with g, labeled I, II, and III by increasing alignment sensitivity g. Phase I corresponds to $g < g^*$ and is characterized by exhibiting no macroscopic orientational order. Figure 3 shows that within phase I there is a dynamic phase transition from a spatially homogeneous to an aggregate phase as g is increased. The degree of aggregation is characterized by the average cluster size $\langle k \rangle$,

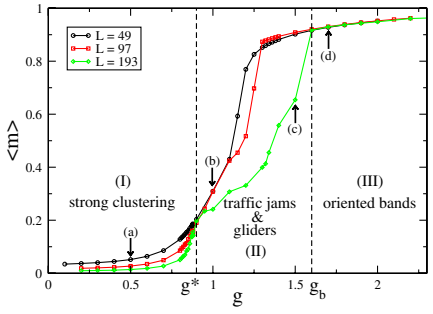

FIG. 2 (color online). Mean orientation $\langle m \rangle$ vs the alignment sensitivity g for systems with density $d = 0.3$ and migration rate $\upsilon_0 = 100$. Simulations were carried out for 2×10^7 time steps. The different curves correspond to different system sizes L. The boundary between phase I and II, g^*, and between phase II and III, g_b, are indicated by the vertical dashed lines. (a) to (d) refer to the simulation snapshots shown in Fig. 1.

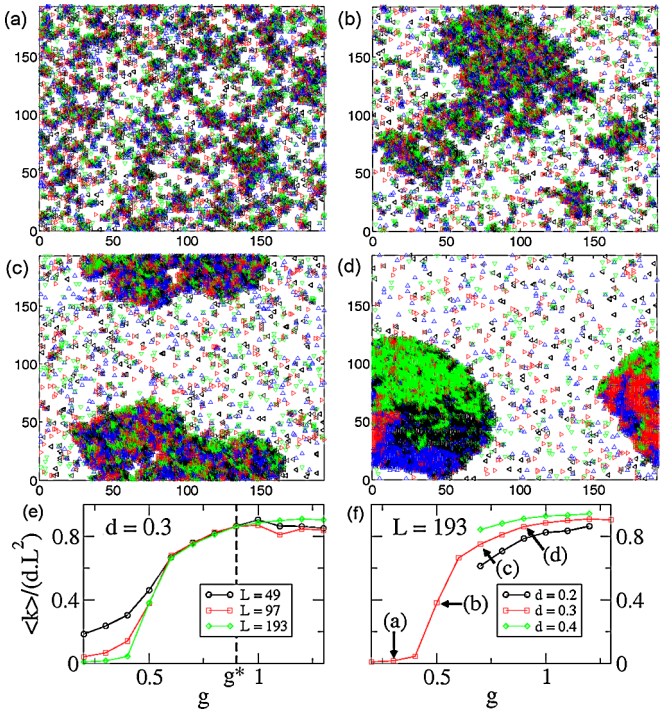

FIG. 3 (color online). Phase transition to aggregation (phase I). (a) to (d) correspond to simulation snapshots whose value of g is indicated in (f) (other parameters as in Fig. 2). The average cluster size $\langle k \rangle$ normalized by the total number of particles, dL^2, as function of g is shown in (e) for various system sizes, and in (f) for various densities.

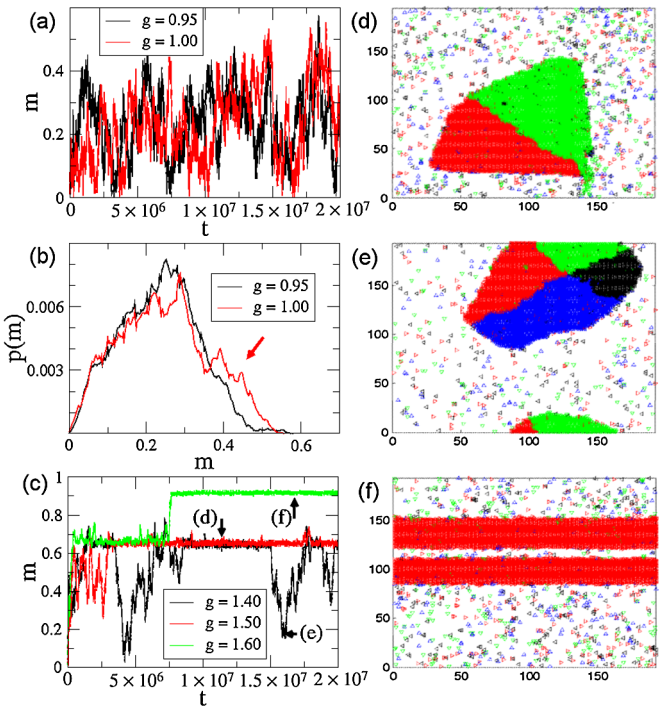

FIG. 4 (color online). Phase transition to orientational order. Time series $m(t)$, histogram, and typical spatial configurations for phase II, $g^* < g \leq g_b$. Letters in (c) indicate simulation snapshots shown in (d)–(f). Parameters as in Fig. 2.

which is computed as the temporal average of $\langle k \rangle = \sum_k k p(k, t)$, with $p(k, t) = k n_k(t)/N$, where $n_k(t)$ is the number of clusters of mass k at time t and $N = dL^2$ is the number of particles in the system. The figure shows that there exists a critical value g_a above which a phase transition to aggregation occurs, with $g_a < g^*$. As g approaches g^*, more than 85% of the particles in the system form a large aggregate. The transition point between phase I and II is at g^*, where the curves $\langle m \rangle(g, L)$ for different system sizes L meet. Interestingly, g^* seems to be independent of the density d, as confirmed with simulations for various system sizes with density $d = 0.2$, 0.3, and 0.4 (data not shown). Moreover, g^* coincides with the critical point for the full occupancy problem, i.e., $d = 1$. Figure 4(a) shows time series of $m(t)$ for values of g close to g^*. The order parameter $m(t)$ exhibits fluctuations between high and low values. Low m-values correspond to the appearance of round traffic jams, while high values correspond to elongated traffic jams where two directions dominate over the other two. Traffic jams results from the jamming of four particle clusters attempting to move to the left, right, upward, and downward, respectively. Fluctuations are due to the competition between these four clusters. Figure 4(b) shows that the distributions $p(m)$ obtained from the $m(t)$ time series for values of g close to g^* do not exhibit a Gaussian shape as expected for a second-order transition, but rather a bimodal distribution (the arrow indicates the second peak) as expected for first-order transitions. The coexistence of several particle configurations (or "phases") exhibiting different degrees of ordering, i.e., values of m, is evident for values of g deep into phase II. Figure 4(c) shows that $m(t)$ jumps between well-defined values corresponding to different spatial patterns. Values of $m(t) \sim 1/\sqrt{2}$ are associated to gliders, while higher values of $m(t)$ correspond to bands. Lower values of $m(t)$ are due to the presence of traffic jams. Gliders are dynamical traffic jams moving backwards with respect to their average orientation. Their presence affects the temporal evolution of the center of mass of the system, $\mathbf{x}_{\mathrm{cm}}(t)$, which exhibits ballistic motion whenever there is a glider, while otherwise is Brownian. As result of this, the average speed of the center of mass $\langle V_{\mathrm{cm}} \rangle$ peaks at values of g where gliders are more stable [23]; see Fig. 5. Gliders are remarkably different from traffic jams observed in 2D traffic models [24], arguably due to the presence of the alignment mechanism, Eq. (1). How frequently gliders appear and for how long they survive, depends on the value of g and L. For example, for $g = 1.4$, $m(t)$ displays excursions from low to high values that reflect the fact the system alternates between traffic jams and gliders. For an illustration of this dynamics, see [25]. For $g > g_b$, i.e., in phase III, the only stable configurations is a band. In contrast to g^*, g_b is highly dependent on L.

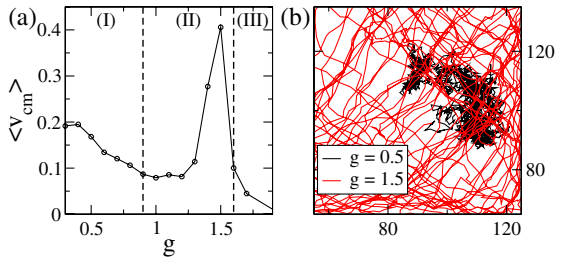

FIG. 5 (color online). (a) average speed of the center of mass $\langle V_{\mathrm{cm}} \rangle$ as function of g. (b) Trajectories of the center of mass for two different values of g.

Discussion.— In the limit of full occupancy, $d = 1$, particles are frozen in their positions and the only action allowed to them is reorientation. The system defined by Eqs. (1) and (2) becomes an equilibrium system in this limit, whose order is again characterized by $m(t)$. Since, by definition, there are only four possible orientations, we can safely claim that the model reduces to a 4-state planar Potts model [19]. It has been shown that this model can be reduced to the standard 2-Potts model [20]. In two-dimensions, the standard q-Potts model exhibits a continuous transition for $q \leq 4$, and a discontinuous one for $q > 4$ [19]. Thus, our model exhibits a second-order transition for $d = 1$, as confirmed via simulations (data not shown). For $v_0 > 0$ and $d < 1$, we are in a pure nonequilibrium scenario. The migration rule, Eq. (2), breaks detailed balance and prevents us from writing down a free energy. Nevertheless, it is worth to compare our system with its equilibrium counterpart, the diluted Potts model with annealed vacancies. If we represent the absence of particles in a lattice position with an extra vector direction, we end up with a 5-Potts system with full occupancy, instead of a diluted 4-Potts system. In consequence, according to what was said above, the transition would be first-order. The argument applies to the standard Potts model and assumes vacancies are in thermal equilibrium, which is not true for Eq. (2). Nevertheless, it helps to realize that a discontinuous dynamic phase transition is quite possible in our nonequilibrium system.

In summary, we have shown through a minimal model that volume exclusion effects, when they are allowed to stop particle motion, can lead to a surprisingly rich variety of self-organized patterns. Such effects introduce a coupling between local density, local orientation and particle speed that strongly affects the large-scale behavior of the system, with the jamming of particles playing a dominant role. This coupling is present in many real systems as in gliding bacteria, animal groups, etc. Certainly, several features of the self-organized patterns described here depend on the discrete nature of the model. Nevertheless, we expect similar phenomena to emerge in off-lattice, continuum symmetry systems. For instance, static traffic jams are probably a robust property of all systems where stagnation can occur. Here we have also learned that the jamming of self-propelled particles can lead to unexpected self-organized structures in two-dimensions like dynamical traffic jams, e.g., gliders. The presence of an alignment mechanism induces (local) orientational order, and provided particles are oriented, density waves of stagnated particles should emerge. The results reported here are a first step toward an understanding of the possible phenomena that such a coupling may induce.

We thank A. Greven and C. F. Lee for useful comments.

[1] D. Helbing, I. Farkas, and T. Vicsek, Nature (London) **407**, 487 (2000).
[2] A. Cavagna *et al.*, Proc. Natl. Acad. Sci. U.S.A. **107**, 11 865 (2010).
[3] K. Bhattacharya and T. Vicsek, New J. Phys. **12**, 093019 (2010).
[4] J. Buhl *et al.*, Science **312**, 1402 (2006).
[5] P. Romanczuk, I. D. Couzin, and L. Schimansky-Geier, Phys. Rev. Lett. **102**, 010602 (2009).
[6] H. P. Zhang *et al.*, Proc. Natl. Acad. Sci. U.S.A. **107**, 13 626 (2010).
[7] V. Schaller *et al.*, Nature (London) **467**, 73 (2010).
[8] V. Narayan, S. Ramaswamy, and N. Menon, Science **317**, 105 (2007).
[9] A. Kudrolli *et al.*, Phys. Rev. Lett. **100**, 058001 (2008); A. Kudrolli, Phys. Rev. Lett. **104**, 088001 (2010).
[10] J. Deseigne, O. Dauchot, and H. Chaté, Phys. Rev. Lett. **105**, 098001 (2010).
[11] T. Vicsek *et al.*, Phys. Rev. Lett. **75**, 1226 (1995).
[12] G. Grégoire and H. Chaté, Phys. Rev. Lett. **92**, 025702 (2004).
[13] F. Peruani, A. Deutsch, and M. Bär, Eur. Phys. J. Special Topics **157**, 111 (2008); F. Ginelli *et al.*, Phys. Rev. Lett. **104**, 184502 (2010).
[14] H. Chaté, F. Ginelli, and R. Montagne, Phys. Rev. Lett. **96**, 180602 (2006).
[15] H. J. Bussemaker, A. Deutsch, and E. Geigant, Phys. Rev. Lett. **78**, 5018 (1997).
[16] Z. Csahók and T. Vicsek, Phys. Rev. E **52**, 5297 (1995).
[17] O. J. O'Loan and M. R. Evans, J. Phys. A **32**, L99 (1999).
[18] J. R. Raymond and M. R. Evans, Phys. Rev. E **73**, 036112 (2006).
[19] F. Y. Wu, Rev. Mod. Phys. **54**, 235 (1982).
[20] D. D. Betts, Can. J. Phys. **42**, 1564 (1964).
[21] D. T. Gillespie, J. Phys. Chem. **81**, 2340 (1977).
[22] T. Klauss and A. Voss-Boehme, in *Mathematical Modeling of Biological Systems* (Birkhauser, Boston, 2008), Vol. II, p. 353.
[23] $\langle V_{\mathrm{cm}} \rangle$ has been computed as $\langle V_{\mathrm{cm}} \rangle = \langle |\mathbf{x}_{\mathrm{cm}}(t + \tau) - \mathbf{x}_{\mathrm{cm}}(t)|/\tau \rangle_t$, with $\tau = 10^4$ and $\langle \ldots \rangle$ a temporal average.
[24] O. Biham, A. A. Middleton, and D. Levine, Phys. Rev. A **46**, R6124 (1992); T. Nagatani, Phys. Rev. E **48**, 3290 (1993).
[25] See supplemental material at http://link.aps.org/supplemental/10.1103/PhysRevLett.106.128101 for a movie.